

Isotropic myosin-generated tissue tension is required for the dynamic orientation of the mitotic spindle

Maxine S. Y. Lam^a, Ana Lisica^{b,c}, Nitya Ramkumar^a, Ginger Hunter^a, Yanlan Mao^{a,c}, Guillaume Charras^{b,c,d}, and Buzz Baum^{a,c,*}

^aMRC Laboratory for Molecular Cell Biology, ^bLondon Centre for Nanotechnology, ^cInstitute for the Physics of Living Systems, and ^dDepartment of Cell and Developmental Biology, University College London, London WC1E 6BT, United Kingdom

ABSTRACT The ability of cells to divide along their longest axis has been proposed to play an important role in maintaining epithelial tissue homeostasis in many systems. Because the division plane is largely set by the position of the anaphase spindle, it is important to understand how spindles become oriented. While several molecules have been identified that play key roles in spindle orientation across systems, most notably Mud/NuMA and cortical dynein, the precise mechanism by which spindles detect and align with the long cell axis remain poorly understood. Here, in exploring the dynamics of spindle orientation in mechanically distinct regions of the fly notum, we find that the ability of cells to properly reorient their divisions depends on local tissue tension. Thus, spindles reorient to align with the long cell axis in regions where isotropic tension is elevated, but fail to do so in elongated cells within the crowded midline, where tension is low, or in regions that have been mechanically isolated from the rest of the tissue via laser ablation. Importantly, these differences in spindle behavior outside and inside the midline can be recapitulated by corresponding changes in tension induced by perturbations that alter nonmuscle myosin II activity. These data lead us to propose that isotropic tension within an epithelium provides cells with a mechanically stable substrate upon which localized cortical motor complexes can act on astral microtubules to orient the spindle.

Monitoring Editor

Manuel Théry
CEA, Hôpital Saint-Louis

Received: Oct 1, 2019

Revised: Feb 19, 2020

Accepted: Apr 14, 2020

INTRODUCTION

When an epithelial cell undergoes a symmetric division, spindles tend to orient so that they divide along the long cell axis. This process, often known as the long-axis or Hertwig's rule (Hertwig 1896;

This article was published online ahead of print in MBoC in Press (<http://www.molbiolcell.org/cgi/doi/10.1091/mbc.E19-09-0545>) on April 22, 2020.

Author contributions: B.B. and M.L. designed the experiments; M.L., N.R., and G.H. conducted the experiments; M.L., A.L., and G.H. analyzed the data; B.B., G.C., M.L., and A.L. wrote the paper; G.C. and Y.M. advised on the experiments and paper.

*Address correspondence to: Buzz Baum (b.baum@ucl.ac.uk).

Abbreviations used: AP, after pupariation; CFP, cumulative frequency plot; GFP, green fluorescent protein; IR, interfering RNA; ML, midline; MTs, microtubules; NEB, nuclear envelope breakdown; OML, outside midline; RFP, red fluorescent protein; TCJs, tricellular junctions; WT, wild-type.

© 2020 Lam et al. This article is distributed by The American Society for Cell Biology under license from the author(s). Two months after publication it is available to the public under an Attribution–Noncommercial–Share Alike 3.0 Unported Creative Commons License (<http://creativecommons.org/licenses/by-nc-sa/3.0>). "ASCB®," "The American Society for Cell Biology®," and "Molecular Biology of the Cell®" are registered trademarks of The American Society for Cell Biology.

Wilson 1925; Gibson and Gibson 2009; Minc and Piel 2012; Campinho et al. 2013; Mao et al. 2013; di Pietro et al., 2016), has been suggested to play important roles in reducing the variance in cell packing and in aiding the relaxation of tissues subjected to mechanical strain (Gibson and Gibson 2009; Mao et al. 2011; Campinho et al., 2013; Wyatt et al., 2015; Bosveld et al., 2016). While this behavior has been observed in many experimental model systems, the precise cellular and tissue level cues used to orient the spindles and to direct oriented cell divisions remain poorly understood. To shed light on this process, here we use the fly notum as a model system in which to explore how spindle rotation is influenced by tissue mechanics and mitotic cell shape.

In the notum, as in many other systems (Grill and Hyman 2005; Wühr et al., 2010; Kimura and Kimura 2011; Minc et al., 2011; Kotak and Gönczy 2013; Bosveld et al., 2016), spindles are positioned by forces generated by cortically localized dynein as it binds close to the plus ends of astral microtubules (MTs) and walks toward MT minus ends. In mitotic epithelial cells, this cortical Dynein is

associated with Mud/NuMA/LIN-5 (Bosveld *et al.*, 2016; di Pietro *et al.*, 2016; Gloerich *et al.*, 2017) at the cell cortex (Dujardin and Vallee 2002; Kotak and Gönczy 2013; di Pietro *et al.*, 2016; Kraft and Lackner, 2017), and drives changes in spindle orientation. Our understanding of the mechanisms that translate the activity and distribution of Mud/NuMA-associated motor complexes into the ability of mitotic spindles to read and orient themselves relative to the long cell axis, however, remains incomplete.

In a study looking at the rules that govern spindle alignment relative to the long cell axis in the developing fly notum, Mud/NuMA was found enriched at tricellular junctions (TCJs; where three or more cells come into contact) during interphase, and was seen remaining in place during entry into mitosis (Bosveld *et al.*, 2016). This led the authors to propose that TCJ-associated Mud/NuMA functions as a memory of interphase cell shape that is read by the spindle in mitosis (Bosveld *et al.*, 2016). In support of this idea, a model based on TCJs was able to match experimentally measured average spindle orientation to within 30° (Bosveld *et al.*, 2016). While these data support TCJ-localized Mud/NuMA playing a role in directing the orientation of spindles relative to the interphase long cell axis, the fairly low accuracy of predictions based upon the distribution of TCJs suggests that the process is noisy and/or responsive to other inputs. Moreover, in other tissues and other model epithelia, Mud/NuMA does not appear to preferentially localize to TCJs (Radulescu and Cleveland, 2010; Dimitracopoulos *et al.*, 2016; Gloerich *et al.*, 2017; Hart *et al.*, 2017; Nestor-Bergmann *et al.*, 2017; Finegan *et al.*, 2018; Heppert *et al.*, 2018; Scarpa *et al.*, 2018; Tang *et al.*, 2018). This implies roles for additional factors. Previous work has suggested roles for cell shape and physical force (Théry *et al.*, 2005, 2006, 2007). Specifically, anisotropic mechanical tension applied to the cell has been shown to be sufficient to guide mitotic spindle orientation in isolated cells in culture (Fink *et al.*, 2011) and in epithelial tissues subjected to an applied tension axis (Mao *et al.*, 2011; Campinho *et al.*, 2013; Nestor-Bergmann *et al.*, 2017; Scarpa *et al.*, 2018; Tang *et al.*, 2018). In addition, spindles have been shown to rapidly reorient in response to changes in mitotic cell shape (O'Connell and Wang, 2000; Minc *et al.*, 2011).

More work, however, is required to determine how external physical force and cell shape combine to influence spindle movements and oriented divisions. While *in vitro* systems allowing application of stretch to an epithelium have yielded key insights into the mechanisms of division orientation, stretching a tissue leads to simultaneous changes in epithelial cell shape, TCJ polarity, and the dominant tension axis, making it hard to determine the relative contribution of these different cues to spindle orientation (Wyatt *et al.*, 2015; Hart *et al.*, 2017; Nestor-Bergmann *et al.*, 2017; Finegan *et al.*, 2018; Scarpa *et al.*, 2018). Also, in some of these instances, spindles appear to follow the change in cell shape that is induced via force rather than the tension axis itself (Wyatt *et al.*, 2015). Here, to better separate these variables, we have used the developing fly notum as a model system in which to compare the behavior of spindles in cells of similar shape in regions of this monolayer epithelium that experience different levels of tension. In this way, we identify a role for isotropic myosin-dependent tissue tension in promoting the effective rotation of spindles toward the long cell axis.

RESULTS

Local crowding reduces the ability of cells to rotate to the long axis

Regional differences in resting tissue tension across the fly notum (Marinari *et al.*, 2012) make it an ideal system in which to study how

tissue mechanics influence cell behaviors. In the crowded midline of the notum (ML), many cells have a well-defined long cell axis at 15 h after pupariation (AP; Figure 1A), while experiencing little isotropic tension (Marinari *et al.*, 2012). By contrast, cells outside of the notum midline (OML) experience relatively high levels of isotropic tension (Marinari *et al.*, 2012; Curran *et al.*, 2017). Within the space of a few hours (by ~19 h AP), the majority of cells both inside and outside the midline then undergo a single round of division. By comparing spindle behavior in dividing elongated cells (which we define as having an aspect ratio >1.2) in these two mechanically distinct regions of the tissue, it is therefore possible to assess how isotropic tissue tension influences spindle rotations and division orientation.

To do so, we followed spindle dynamics and cell shape using Spider-GFP, which labels both the plasma membrane and the nuclear envelope (before loss of the nuclear-cytoplasmic compartment barrier), together with tubulin-mCherry to label spindle microtubules or centrosomin-RFP to label centrosomes (Figure 1B). Using these markers, spindle poles were seen aligning with the plane of the tissue (to within 1.5 μm of one another, often within a single confocal z section) at the very onset of mitosis (measured by the influx of fluorescent signal in to the nuclear region; Figure 1B). Spindles then remained in plane throughout mitosis (Figure 1B), despite undergoing significant rotations in the plane of the tissue (Figure 1B and Supplemental Figure S1L). In parallel, cells in the epithelium were seen rounding up as they entered mitosis (Rosa *et al.*, 2015), as they do in many other animal cell systems (Ramkumar and Baum, 2016). Because the process of mitotic rounding was incomplete in the more elongated cells in the tissue, these cells retained their long cell axis while in mitosis (Supplemental Figure S1, A–C), enabling us to determine how spindles align relative to mitotic cell shape.

In characterizing spindle movements in these two mechanically distinct regions of the same tissue, we were able to make a number of observations. First, while spindles in cells both inside and outside the midline were born with a random orientation (Supplemental Figure S1E; $p = 0.54$ for ML and $p = 0.43$ for OML), by anaphase, the majority had undergone rotational movements that brought them into closer alignment with the long cell axis (Figure 1, C and G; anaphase). Interestingly, however, this ability of spindles to reorient so as to become aligned with the long cell axis proved better in cells outside of the midline than it was within the very elongated cells of the midline (compare Figure 1, C and D and Figure 1, G and H). Thus, while there was a significant overall improvement in the orientation of spindles relative to the long cell axis between nuclear envelope breakdown (NEB) and anaphase in cells outside of the midline (Figure 1D), spindles in cells of the midline failed to undergo a significant large-scale realignment (Figure 1H). Because most models of spindle orientation predict that the cues for long-axis orientation are more accurate as cell shape becomes more anisotropic (Théry *et al.*, 2007; Minc *et al.*, 2011; Corrigan *et al.*, 2015; Bosveld *et al.*, 2016), we found this result surprising. In support of this finding, though, we found no statistically significant correlation between spindle orientation and cell elongation either within or outside of the midline in this tissue (Supplemental Figure S1, C and D).

To better observe the large-scale individual rotational movements that underlie the observed changes in spindle alignment seen at the population level, we also separated the data based upon initial spindle orientation into those oriented to within <45° of the long axis or >45° from the long axis at NEB, reasoning that spindles born furthest from the long axis would need to undergo the

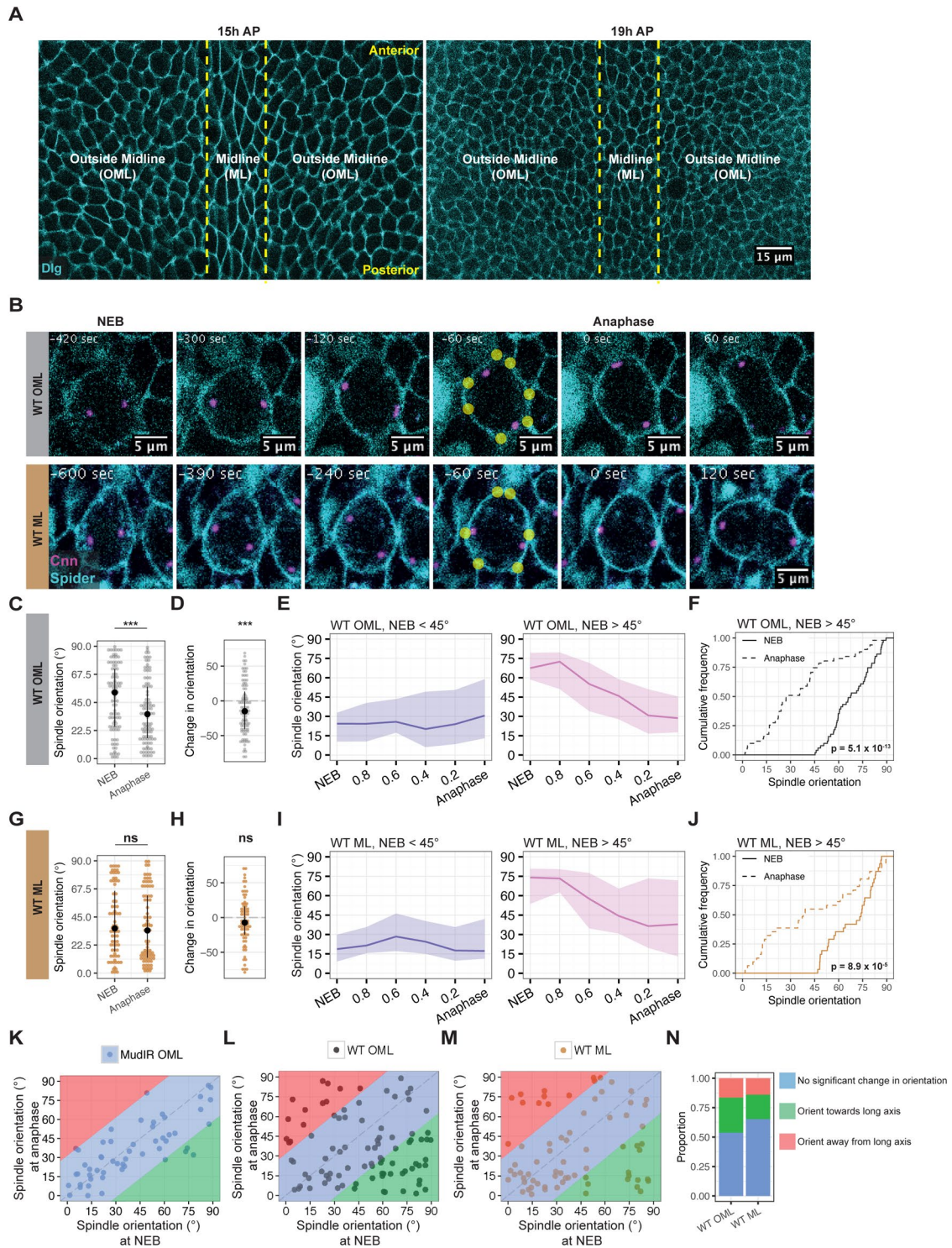


FIGURE 1: (A) *Drosophila notum* at 15 h and 19 h after pupariation (AP). Cell outlines are labeled with Dlg::YFP (cyan). Midline region is indicated with yellow dashed lines. (B) Example WT cell outside the midline (OML) and in the midline (ML) during mitosis. Centrosomes are labeled with centrosomin-RFP (magenta) and cell membranes are labeled with Spider-GFP (cyan). Yellow dots indicate tricellular junctions (TCJs). Cell long axis correlates with TCJ polarity, and spindles (marked by centrosomes) can be seen rotating toward the long cell axis during mitosis in the WT OML example but not in the WT ML example. (C) Spindle orientation at NEB (median = 53.0 $^{\circ}$, IQR = 25.5 $^{\circ}$ –71.7 $^{\circ}$) and anaphase (median = 32.6 $^{\circ}$, IQR = 16.4 $^{\circ}$ –57.5 $^{\circ}$) for WT cells outside the midline. Orientation at anaphase is better than that at NEB ($p = 0.004$, $n = 91$, one-sided Kolmogorov–Smirnov test). (D) Change in spindle orientation from NEB to anaphase for WT cells outside the midline. The overall change in spindle orientation is $-12.1 \pm 3.8^{\circ}$ ($p = 0.002$, $n = 91$, two-sided t test against 0), indicating that spindles have reduced their orientation to the long axis. (E) Spindle orientation over time, normalized from NEB to anaphase for WT spindles outside the midline that are initially oriented <45 $^{\circ}$ (left, purple) or >45 $^{\circ}$ (right, pink) to the long axis. Lines indicate median and shaded region indicates interquartile range. (F) Spindle

largest net movements to come into alignment with the long cell axis at anaphase. Indeed, this proved to be the case. Spindle behavior was found to depend on initial orientation (Figure 1, E and I). Thus, while the subset of spindles born to within $<45^\circ$ of the long cell axis tended to remain relatively closely aligned with the long axis for cells both outside and within the midline (Figure 1, E and I, left panel), spindles born at an angle of $>45^\circ$ relative to the long cell axis underwent larger net rotations during the course of mitosis that were sufficient to bring them into alignment with the long cell axis (Figure 1, E and I, right panel). Again this analysis revealed striking regional differences in spindle behavior: the final angular distribution of the population of spindles borne at an angle $>45^\circ$ to the long cell axis was broader in cells within the midline (Figure 1I, right panel, pink shaded area) than it was for cells outside of the midline (Figure 1E, right panel, pink shaded area). Furthermore, this was not due to local differences in the ability of spindles to rotate (Supplemental Figure S1M). Instead, it reflected regional differences in the ability of spindles to rotate persistently in a directional matter so that by anaphase they end up relatively well-aligned with the long cell axis (compare Figure 1, F and J).

Spindle movement is dependent on Mud/NuMA

Mud/NuMA is a key conserved regulator of spindle orientation (di Pietro *et al.*, 2016), and has been previously shown to be involved in the notum in spindle rotation and orientation to the TCJ axis, which coincides with the long cell axis in elongated cells (Bosveld *et al.*, 2016). To determine whether Mud/NuMA was required for the dynamic spindle orientation observed in our experiments, we used RNA interference (IR) to silence its expression (Supplemental Figure S1, F and M–P). When quantifying spindle rotational motion under these conditions, we excluded cells with z-positioning defects and focused instead on Mud-IR spindles that had aligned with the plane of the tissue. At mitotic entry, these spindles had an orientation that was random, as it was in the control (Supplemental Figure S1F, NEB curve; $p = 0.44$, compared with random). But in contrast to the control, Mud-IR spindles did not undergo a significant change in orientation during the course of mitosis (Supplemental Figure S1, F and N–P). In fact, in contrast to all other conditions tested, spindles in Mud-IR cells appeared unable to undergo any significant rotational movements (Supplemental Figure S1M). These data enabled us to define a threshold above which spindle motion could be assumed

to be directed by the Mud/NuMA-dependent machinery previously implicated in spindle positioning in this and other systems (i.e., spindles with a net rotation or change in orientation $>90\%$ of that in Mud-IR tissues; Figure 1, K–N, red and green regions). Using this as a cutoff, we again observed a larger proportion of spindles undergoing Mud/NuMA-dependent rotations toward the long axis in cells outside the midline compared with spindles within the midline region (Figure 1, L–N, green area). Taken together, these data indicate that spindle movement in the notum differs between mechanically distinct regions of the tissue, and is a dynamic and directed process that requires Mud/NuMA.

Tissue tension and myosin activity influence spindle orientation

As previous work has shown that isotropic tension in the notum midline is lower than it is outside of the midline, these data suggested a potential role for regional differences in tissue mechanics in directed spindle rotation. To explore this idea further, we tested how the expression of a phospho-dead version of myosin light chain (Spaghetti squash, Sqh), SqhAA, would influence spindle rotation (Winter *et al.*, 2001; Curran *et al.*, 2017). For this analysis we focused on cells outside of the midline, where tension is normally relatively high and used laser ablation to show that this treatment is sufficient to reduce tissue tension as assessed by junctional recoil (Supplemental Figure S2A). As an alternative strategy, we also used RNAi to silence the expression of Rho kinase (ROK), an activator for Sqh (Amano *et al.*, 1996; Mizuno *et al.*, 1999), to reduce tension in the notum (Curran *et al.*, 2017). Importantly, for this analysis, neither treatment visibly altered the extent of mitotic rounding and did not perturb the ability of spindles to position themselves within the plane of the tissue. Furthermore, the orientation of spindles at NEB was not affected by expression of SqhAA or ROK-IR (Supplemental Figure S2C). However, both treatments compromised the ability of spindles to dynamically orient to the long cell axis, with ROK-IR expression having a stronger effect (Figure 2, A and B). In fact, the loss of tissue tension induced by these treatments caused spindles in cells outside of the midline to behave like spindles in the wild-type (WT) midline (compare Figure 1I to Figure 2, C and E, and proportions in Figure 2I). This is consistent with our hypothesis that regional-specific differences in tissue tension result in differences in local spindle behavior. Once again, these changes could not be attributed to a loss in the ability

orientations at NEB (median = 67.5° , IQR = 58.6° – 79.3°) and anaphase (median = 28.6° , IQR = 17.6° – 45.5°) for WT OML spindles with an orientation of $>45^\circ$ at NEB plotted as cumulative frequency plot (CFP). Orientation at anaphase is much better than that at NEB ($p = 5.1 \times 10^{-13}$, $n = 51$, one-sided Kolmogorov–Smirnov test). (G) Spindle orientation at NEB (median = 35.9° , IQR = 17.3° – 65.9°) and anaphase (median = 34.3° , IQR = 12.5° – 62.2°) for WT cells in the midline. Orientation at anaphase is similar that at NEB ($p = 0.1$, $n = 72$, one-sided Kolmogorov–Smirnov test). (H) Change in spindle orientation from NEB to anaphase for WT cells in the midline. The overall change in spindle orientation is $-5.3 \pm 4.0^\circ$ ($p = 0.2$, $n = 72$, two-sided t test against 0), indicating that spindles have not changed their orientation. (I) Spindle orientation over time, normalized from NEB to anaphase for WT spindles in the midline that are initially oriented $<45^\circ$ (left, purple) or $>45^\circ$ (right, pink) to the long axis. Lines indicate median and shaded region indicates interquartile range. (J) Spindle orientation at NEB against spindle orientation at anaphase for Mud-IR OML cells. Distribution of orientations on the graph were used to define regions where there was no significant change in orientation (blue), where spindles oriented toward the long axis (green), and where spindles oriented away from the long axis (red). (K) Spindle orientations at NEB (median = 74.0° , IQR = 53.7° – 80.8°) and anaphase (median = 37.8° , IQR = 13.1° – 71.8°) for WT ML spindles with an orientation of $>45^\circ$ at NEB plotted as CFP. Orientation at anaphase is lower than that at NEB ($p = 8.9 \times 10^{-5}$, $n = 31$, one-sided Kolmogorov–Smirnov test). Compare p value to that in F. (K) Spindle orientation at NEB against spindle orientation at anaphase for Mud-IR OML cells. Blue region contains 90% of Mud-IR data; green regions indicate spindles that have changed orientation toward the long axis; red regions indicate spindles that have changed orientation away from the long axis. (L) Spindle orientation at NEB against spindle orientation at anaphase for WT OML cells. Colored regions indicate regions as defined in K. (M) Spindle orientation at NEB against spindle orientation at anaphase for WT ML cells. Colored regions indicate regions as defined in K. (N) Proportions of WT OML and ML spindles that fall into categories as defined in K.

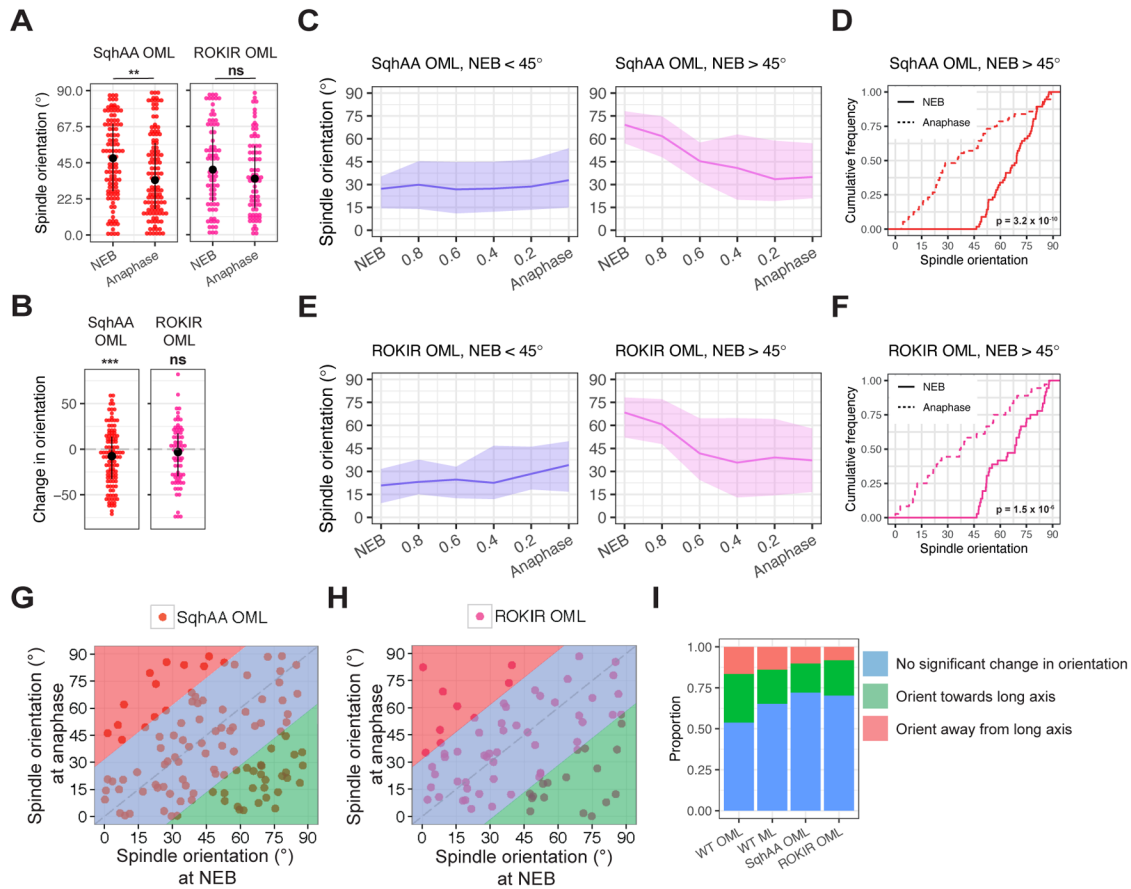


FIGURE 2: A: Spindle orientation at NEB and anaphase for SqhAA and ROK-IR cells outside the midline. SqhAA, NEB: median = 47.9°, IQR = 27.4°–69.2°; SqhAA, anaphase: median = 34.3°, IQR = 16.2°–57.3°. ROK-IR, NEB: median = 40.6°, IQR = 20.4°–67.3°; ROK-IR, anaphase: median = 35.0°, IQR = 16.5°–55.4°. Orientation at anaphase is better than that at NEB for SqhAA OML cells ($p = 0.007$, $n = 109$, one-sided Kolmogorov–Smirnov test), but orientation at anaphase is similar to that at NEB for ROK-IR OML cells ($p = 0.3$, $n = 74$, one-sided Kolmogorov–Smirnov test). (B) Change in spindle orientation from NEB to anaphase for SqhAA and ROK-IR cells outside the midline. The overall change in spindle orientation is $-9.1 \pm 3.0^\circ$ for SqhAA OML cells ($p = 0.004$, $n = 109$, two-sided t test against 0) and $-6.0 \pm 3.7^\circ$ for ROK-IR OML cells ($p = 0.1$, $n = 74$, two-sided t test against 0). (C) Spindle orientation over time, normalized from NEB to anaphase for SqhAA spindles outside the midline that are initially oriented $<45^\circ$ (left, purple) or $>45^\circ$ (right, pink) to the long axis. Lines indicate median and shaded region indicates interquartile range. (D) Spindle orientations at NEB (median = 69.2°, IQR = 57.1°–78.1°) and anaphase (median = 34.9°, IQR = 21.0°–57.0°) for SqhAA OML spindles with an orientation of $>45^\circ$ at NEB plotted as CFP. Orientation at anaphase is better than that at NEB ($p = 3.2 \times 10^{-10}$, $n = 56$, one-sided Kolmogorov–Smirnov test). Compare p value to that in Figure 1F. (E) Spindle orientation over time, normalized from NEB to anaphase for ROK-IR spindles outside the midline that are initially oriented $<45^\circ$ (left, purple) or $>45^\circ$ (right, pink) to the long axis. Lines indicate median and shaded region indicates interquartile range. (F) Spindle orientations at NEB (median = 68.4°, IQR = 52.2°–78.2°) and anaphase (median = 37.2°, IQR = 16.6°–58.0°) for ROK-IR OML spindles with an orientation of $>45^\circ$ at NEB plotted as CFP. Orientation at anaphase is better than that at NEB ($p = 1.5 \times 10^{-6}$, $n = 36$, one-sided Kolmogorov–Smirnov test). Compare p value to that in Figure 1F. (G) Spindle orientation at NEB against spindle orientation at anaphase for SqhAA OML cells. Colored regions indicate regions as defined in Figure 1K. (H) Spindle orientation at NEB against spindle orientation at anaphase for ROK-IR OML cells. Colored regions indicate regions as defined in Figure 1K. (I) Proportions of WT, SqhAA, and ROK-IR OML spindles that fall into categories defined in Figure 1K.

of spindles to move or to undergo rotational movements (Supplemental Figure S2B). Instead, SqhAA and ROK-IR expression impaired the ability of spindles born far from the long axis ($>45^\circ$) to reorient toward the long axis (compare Figure 1, C and E, right panel, pink shaded area, and Figure 1, D and F, p values, to Figure 1, D and F). Note that the effect of these perturbations was even more evident when we categorized spindles based on their ability to reorient relative to the Mud-IR (Figure 1J and Figure 2, E–G), as indicated by a decrease in the proportion of spindles that changed their orientation toward the long cell axis at anaphase (Figure 2, G–I).

Together, these data suggest that tissue tension enhances the ability of spindles to undergo the directed rotation needed to bring them into alignment with the long cell axis. If this hypothesis is correct, it should be possible to rescue the defects in spindle alignment in the tissue midline using genetic perturbations that increase tissue tension by expressing a phosphomimetic version of Sqh, SqhEE (Supplemental Figure S2A). As with the other perturbations, SqhEE expression did not alter the initial orientation of spindles relative to the long cell axis ($p = 0.6$ compared with random), and they were similar to those seen in the WT (Supplemental Figure S3B). However,

SqhEE expression led to a dramatic and significant improvement in overall spindle orientation during the course of mitosis relative to the WT control (Figure 3A), something that was evident for cells both inside and outside of the midline (Supplemental Figure S3, D and E). This was accompanied by a significant increase in the ability of individual spindles to rotate toward the long axis (Figure 3B), and was reflected by an increase in the proportion of spindles that reoriented toward the long axis (Figure 3, C and D, green bars), together with a decrease in the proportion of spindles that reoriented away from the long axis (Figure 3, C and D, red bars). Again, these changes were not due to changes in the overall ability of spindles to rotate (Supplemental Figure S3, A and B). Instead, spindles in SqhEE-expressing tissues that were born misoriented relative to the long axis underwent rotational movements that were more directed than those observed in the WT, bringing them into good alignment with the long cell axis by anaphase (Figure 3E). Taken together, these data support our hypothesis that the relatively poor ability of spindles within cells of the WT midline to reorient during mitosis is a result of the low regional tissue tension due to crowding (Marinari *et al.*, 2012), something that can be restored by changing myosin-dependent tissue tension.

As a further test of the role of tissue mechanics in this system, we wanted to determine how a sudden loss of local isotropic tissue tension would influence spindle orientation. To do so, we used laser ablation to mechanically isolate individual dividing cells from the rest of the tissue by cutting surrounding adherens junctions, to avoid neighboring junctions and potential damage to the dividing cells being analyzed (Figure 3, F and G). We used SqhEE-expressing *nota* for this analysis, where spindle movements toward the long cell axis are more directed and consistent. As a control, we imaged SqhEE-expressing mitotic cells in areas away from the sites of ablation and in *nota* where we did not perform laser ablation.

Because cells about to enter mitosis were identified manually before setting up the ablation, we were unable to capture entry into mitosis in these experiments. We were, however, able to follow spindle rotational movements relative to the long cell axis in these cells as they progressed through mitosis. In the period imaged, both control and mechanically isolated cells underwent similar rotational movements (Supplemental Figure S3D). However, while spindles in control SqhEE cells underwent a significant net change in orientation in the period from the start of observation until anaphase (Figure 3, H and I), spindles in cells that had been mechanically isolated from the surrounding tissue by laser ablation did not (Figure 3, H and I). Despite the small number of cells, spindles that underwent significant rotational movements were clearly observed reorienting toward the long axis by anaphase in control tissues, while such correctional movements were reduced in cells that had been mechanically isolated from their neighbors by laser ablation (Figure 3I).

These data show that spindles change the way they rotate depending on the mechanical environment in which cells find themselves in, as was previously shown for isolated cells in culture (O'Connell and Wang, 2000; Fink *et al.*, 2011). In addition, while myosin perturbations are likely to affect the mitotic cortex, the effects of mechanically isolating a mitotic cell support a role for myosin-dependent isotropic tissue tension at the level of adherens junctions in supporting effective spindle rotation toward the long cell axis.

DISCUSSION

The role of tissue tension in spindle orientation remains a topic of intense investigation. While some studies have suggested that the ability of tissue-scale forces to influence spindle orientation are an indirect consequence of the impact of tension on cell shape

(Mao *et al.*, 2011; Campinho *et al.*, 2013; Wyatt *et al.*, 2015; Nestor-Bergmann *et al.*, 2017), others have pointed to more direct roles for axial tension itself (Théry *et al.*, 2006; Fink *et al.*, 2011; Machicoane *et al.*, 2014; Gloerich *et al.*, 2017; Finegan *et al.*, 2018; Scarpa *et al.*, 2018). However, to our knowledge, a role for isotropic tension in this process has never been examined. Here, by comparing spindle orientation in elongated cells within different mechanical environments, we have unambiguously identified a role for isotropic tissue tension in the dynamic rotation of spindles to the long axis in an epithelium, as expected if spindles within an epithelium continually read and respond to their mechanical environment, as has been previously described for cells in culture (O'Connell and Wang, 2000; Fernandez *et al.*, 2011; Fink *et al.*, 2011; Minc *et al.*, 2011).

More specifically, our analysis reveals that the ability of spindles to undergo a net rotation that brings them into alignment with the long cell axis is less efficient in cells of the crowded midline than it is for cells outside of the midline, even though cells within the midline tend to be the most elongated. Consistent with this being due to regional differences in tissue tension, a reduction in tissue tension (due either to an overall reduction in myosin II activity or the sudden mechanical isolation of mitotic cells) reduced the efficiency of spindle rotation toward the long cell axis. More surprisingly still, in the converse experiment, a perturbation that increased myosin activity in the tissue midline improved the ability of spindles to rotate to align with the long cell axis.

Our analysis supports a growing body of work suggesting that mechanical tension influences spindle orientation (Fink *et al.*, 2011; Gloerich *et al.*, 2017; Hart *et al.*, 2017; Finegan *et al.*, 2018; Scarpa *et al.*, 2018). While previous studies explored a role for anisotropic tension in "overriding" cell shape cues in spindle orientation, our study finds that isotropic tissue tension is important for spindles to correctly read cell shape as a cue.

How might isotropic tissue tension promote persistent spindle rotation to the long axis? In single cells in culture, the mitotic cortex is polarized as the cell rounds up against the tension exerted by retraction fibers on the mitotic body (Théry *et al.*, 2007; Fink *et al.*, 2011; Machicoane *et al.*, 2014; Oakes *et al.*, 2014; Matsumura *et al.*, 2016), and changes in cortical stiffness during mitotic rounding also affect spindle movements (Carreno *et al.*, 2008). Because the overall cortical tension increases when cells round up in a tensile environment (Oakes *et al.*, 2014), this then provides astral microtubules with a stable physical platform upon which to pull and exert torque on the spindle (Redemann *et al.*, 2010), leading to effective spindle rotation toward the long axis. In a tissue, TCJs subjected to isotropic tension may act in a similar way to retraction fibers in a cultured cell on a rigid substrate, exerting tension on the mitotic cell. At the same time, the mitotic cortex provides a physical substrate upon which cortically anchored dynein motors can pull on microtubules to reorient the spindle. Conversely, in crowded tissues, the reduced levels of resting isotropic tissue tension compromises directed spindle rotation. Notably, similar mechanisms could be used to bias spindle orientation in cases where there was a clear axis of tension in the tissue. However, further work will be necessary to confirm this hypothesis.

Strikingly, as we show here, the capacity for directed spindle orientation does not appear to be optimized in the WT notum, because the hyperactivation of myosin can improve the efficiency of spindle rotation to the long axis. This was especially evident in the crowded fly midline, where tissue tension is normally low, even though these cells are among the most elongated in the notum. Thus, although previous studies suggested that the ability of spindles to orient along the long cell axis is important to orient divisions for optimized cell packing (Gibson *et al.*, 2011; Bosveld *et al.*, 2016)

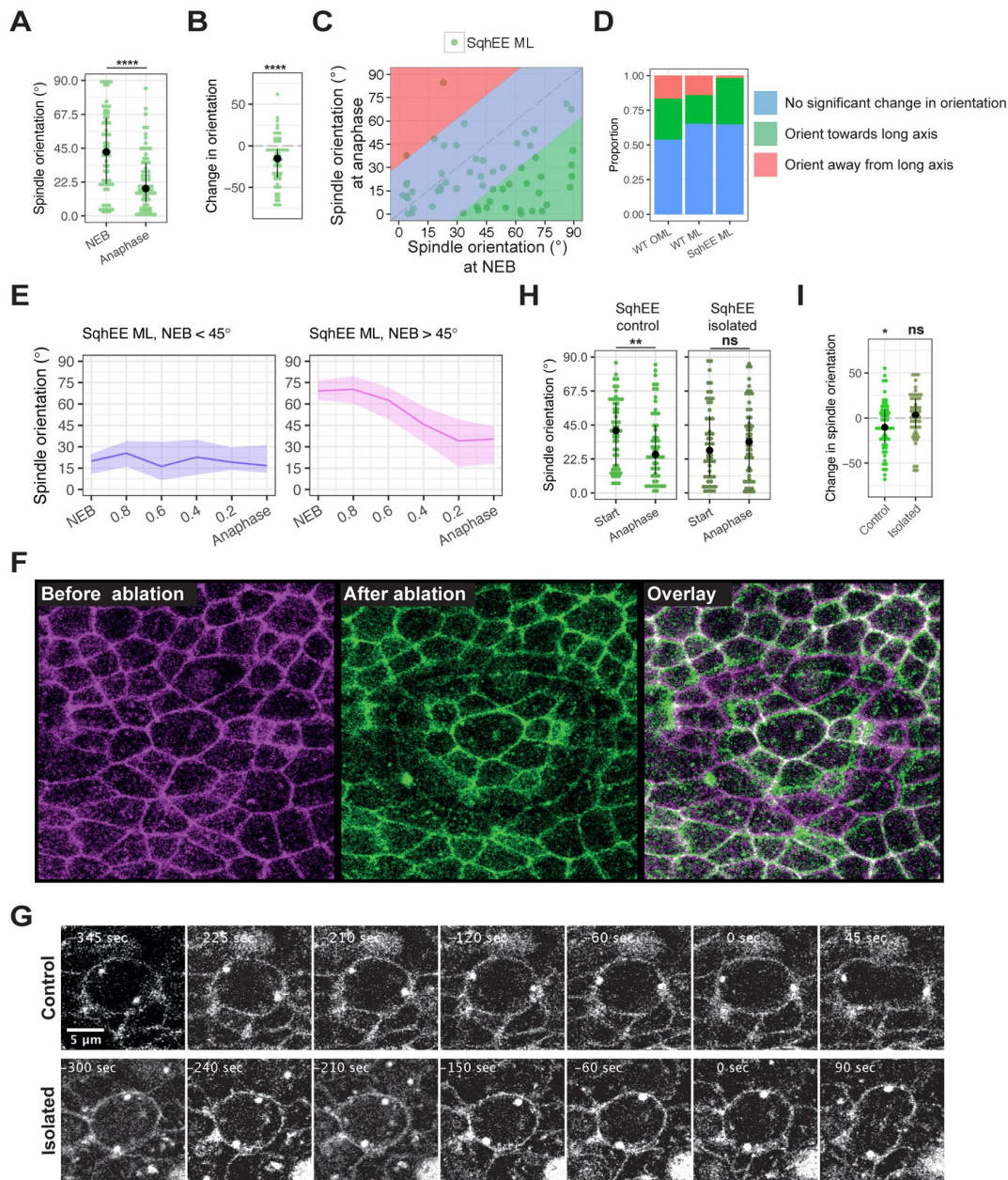


FIGURE 3: A: Spindle orientation at NEB (median = 42.6°, IQR = 21.2°–65.3°) and anaphase (median = 18.2°, IQR = 9.0°–35.0°) for SqhEE ML cells. Orientation at anaphase is better than that at NEB ($p = 0.0002$, $n = 60$, one-sided Kolmogorov–Smirnov test). (B) Change in spindle orientation from NEB to anaphase for SqhEE ML cells. The overall change in spindle orientation is $-19.3 \pm 3.6^\circ$ ($p = 4 \times 10^{-6}$, $n = 60$, two-sided t test against 0), indicating that spindles have rotated toward the long axis. (C) Spindle orientation at NEB against spindle orientation at anaphase for SqhEE ML cells. Colored regions indicate regions as defined in Figure 1K. (D) Proportions of WT and SqhEE ML spindles that fall into categories as defined in Figure 1K. (E) Spindle orientation over time, normalized from NEB to anaphase for SqhEE ML spindles that are initially oriented $<45^\circ$ (left, purple) or $>45^\circ$ (right, pink) to the long axis. Lines indicate median and shaded region indicates interquartile range. (F) Images of apical plane of tissue expressing SqhEE before and after laser ablation isolation. Ablated region is visible as a dark ring. Overlay shows the amount of recoil in cell junctions at the site of ablation, without affecting the cell shape of the mitotic cell (center). (G) Montage of spindle plane of tissue expressing SqhEE with or without laser ablation isolation. Cell membranes and centrosomes are shown in gray. Spindle rotation to the long axis is visible in control cells, but spindle rotation in isolated cells while present is not toward the long axis. (H) Spindle orientation at NEB and anaphase for control and ablation isolated SqhEE cells. SqhEE control, start: median = 41.3°, IQR = 17.8°–59.7°; SqhEE control, anaphase: median = 25.5°, IQR = 12.1°–45.0°. SqhEE isolated, start: median = 28.2°, IQR = 10.7°–51.1°; SqhEE isolated, anaphase: median = 33.8°, IQR = 13.7°–51.4°. Orientation at anaphase is better than that at NEB for control cells ($p = 0.009$, $n = 54$, one-sided Kolmogorov–Smirnov test), but orientation at anaphase is similar to that at NEB for isolated cells ($p = 0.8$, $n = 52$, one-sided Kolmogorov–Smirnov test). (I) Change in spindle orientation from NEB to anaphase for control and ablation isolated SqhEE cells. The overall change in spindle orientation is $-9.3 \pm 3.6^\circ$ for control cells ($p = 0.02$, $n = 54$, two-sided t test against 0) and $2.2 \pm 3.6^\circ$ for isolated cells ($p = 0.6$, $n = 52$, two-sided t test against 0).

this process contributes little to tissue order in the midline of the notum, where mis-orientated spindles frequently fail to efficiently align along the long cell axis, leading to misoriented divisions. Oriented division is therefore unlikely to play a role in the refinement of cell packing in this tissue. Instead, cell division in the midline generates additional heterogeneities in packing that must be resolved via neighbor exchange (Curran *et al.*, 2017) and live cell delamination (Marinari *et al.*, 2012). In contrast, in regions of the tissue that experience higher levels of resting tension, oriented divisions may help restore homogeneous cell packing and maintain epithelial topology, where neighbor exchange events (Curran *et al.* 2017) and live cell delamination are less frequent (Marinari *et al.*, 2012). These data suggest that the developing notum has alternative and mutually exclusive mechanisms by which to resolve packing heterogeneities, and that the level of tension in a tissue modifies the ways in which cell packing is refined.

MATERIALS AND METHODS

Live imaging

Drosophila pupae were selected at the white prepupal stage, 0 h AP, and imaged at 14.5 h AP for 2–3 h at room temperature. Developmental time was halved when incubated at 29°C, and doubled when incubated at 18°C. Pupae for live imaging were attached to a glass slide ventral side down with double-sided tape between spacers made with small glass coverslips. The pupal case was removed from the dorsal side of the animal and a glass coverslip coated with mineral oil on one side was placed over the spacers, just touching the dorsal tissue of the pupa. The entire setup was placed under the microscope for live imaging (Georgiou and Baum, 2010; Zitserman and Roegiers, 2011).

Imaging was done on Leica SPE and SP5 confocal microscopes with a 63× lens (NA) or 60× lens (NA), respectively.

Fly stocks used

Background and visualising of cell outline and mitotic structures

Stock	Source
w ¹¹¹⁸	BL 3605
w ¹¹¹⁸ ; pnr-GAL4	BL 3039
Spider-GFP	Flytrap insertion (BL 59025)
w ¹¹¹⁸ :: Spider-GFP, pnr-GAL4	Recombined strain of BL 3039 and BL 59025 provided by N. Rodriguez (Francis Crick Institute)
Discs large (Dlg)-YFP	Cambridge Protein Trap Insertion (DGRC 115375)
w ¹¹¹⁸ ; ubi-RFP-Cnn	J. Raff (Dunn School of Pathology, University of Oxford)
actin-GAL4, UAS-mCherry- α -Tubulin	Recombined from BL4414 and BL25774 by N. Rodriguez
w*; UAS-mCherry- α -Tubulin	BL 25774

RNAi-mediated silencing. Interfering RNA transcripts targeting expression of proteins were expressed using the GAL4/ UAS system (Brand and Perrimon, 1993). GAL4 expression was under the control of the *pannier* gene (Pnr-GAL4) (Calleja *et al.*, 2000), restricting GAL4 binding of UAS response elements and subsequent expression of constructs to the central region of the notum. Pupae in RNAi experiments were incubated at 25°C or 29°C from 9–14.5 h AP or

0–14.5 h AP to ensure efficient expression of GAL4. Where lethality was seen under these conditions, pupae were incubated at 18°C from 0–14.5 h AP to reduce the activity of GAL4.

The following fly stocks were used in RNAi-mediated silencing:

Stock	Source
Mushroom body defective (Mud)	BL 35044 (Nakajima <i>et al.</i> , 2011)
Rho Kinase (ROK)	VDRC KK104675

Protein coding constructs. Constructs were expressed using the GAL4/ UAS system (Brand and Perrimon, 1993). GAL4 expression was under the control of the *pannier* gene (Pnr-GAL4; Calleja *et al.*, 2000), restricting GAL4 binding of UAS response elements and subsequent expression of constructs to the central region of the notum. All pupae were incubated at 25°C or 29°C from 9–14.5 h AP or 0–14.5 h AP to ensure efficient expression of GAL4.

Stock	Source
UAS-Sqh ^{AA} / TM6B, Tb	Winter <i>et al.</i> , 2001
UAS-Sqh ^{EE} / TM6B, Tb	Winter <i>et al.</i> , 2001

Mechanical isolation by laser ablation

w¹¹¹⁸; ubi-E-cadherin-GFP; Pnr-Gal4 flies were crossed to UAS-sqh^{AA}, UAS-sqh^{EE}, or w¹¹¹⁸ flies to generate pupae for laser ablation in Supplemental Figure S4, A and B. Ablations were performed with 730-nm multiphoton excitation from a Chameleon-XR Ti-sapphire laser on a Zeiss Axioskop2/LSM510 (AIM; Zeiss). A ~20- μ m linear cut, parallel to the tissue midline, was made at the apical surface, using E-cadherin-GFP as a reference. During ablation and initial recoil, a single Z-slice was acquired every 2 s; postrecoil, a Z-stack was acquired every 30 s for an additional 10 min. At least three E-Cad positive fiducial markers marked by E-cadherin-GFP, proximal to each cut site were tracked postablation and averaged to generate the net displacement and speed during initial recoil.

w¹¹¹⁸; ubi-RFP-Cnn; Spider-GFP, Pnr-Gal4/ UAS-Sqh^{EE} pupae were prepared for live imaging. Cells about to undergo mitosis were visually identified by the presence of centrosomes around the nucleus. The region to be ablated was manually marked at the apical surface, and ablated. Ablation was carried out after the first frame, and imaging continued until anaphase was observed. Z-stack images were acquired in Airyscan mode, every 15 s.

Image analysis

Quantification of cell shape. The medial plane was identified as the plane where the majority of the spindle was located, which was usually the plane with both spindle poles visible. The cell outline in the medial plane was manually marked out in FIJI (<http://fiji.sc/Fiji>). The centroid of the outline was taken as the cell center, while the major length and minor length of the fit ellipse to the outline were taken as the length and width of the cell. The angle of the major length of the fit ellipse was taken as the orientation of the long axis of the cell.

Quantification of spindle movements. Spindle movement was tracked by drawing a line between the visible spindle poles from NEB through to anaphase. Spindle angle, centroid, and length were recorded. Spindles were not considered for analysis if apparent spindle poles were more than 1.5 μ m apart. Spindle measurements were taken with tubulin-mCherry marking the spindle or centrosomin-RFP marking the spindle poles.

Calculations of spindle angles were similar for measurements done with tubulin or centrosomin as a marker, and so the results were pooled.

Identification of mitotic events. Mitotic time was taken as the time from NEB until anaphase onset. NEB was identified as the first time frame when nuclear exclusion of background fluorescent signal disappeared. Anaphase onset was identified in cells expressing tubulin-mCherry as the first time frame when tubulin accumulation toward the spindle poles was observed, ~ 3min before furrow ingression begins. In movies using only centrosomin-RFP as a marker, anaphase onset was taken as the time frame 3 min before furrow ingression begins. Late metaphase was defined as 1 min before anaphase onset.

Statistical analysis and data visualisation

A two-sample Mann-Whitney U test was performed to test for differences between roughly normally distributed data. ANOVA was used to test for differences between more than two samples. A two-sample Kolmogorov-Smirnov test was performed to compare distributions of clearly nonnormally distributed data (i.e., spindle orientations). One-sided tests were used when one population was expected to be lower than the other (i.e., anaphase spindle orientation compared with NEB spindle orientation). Random uniform distributions were generated in R. To test for random distributions, spindle orientations were compared with 100 generated randomly uniform distributions using a two-sided Kolmogorov-Smirnov test, and the average *p* value is reported in the text.

Graphpad Prism and R were used to generate graphs representing the data. Line plots representing median over time, with error bars representing interquartile range (IQR) were generated in Prism. Individual line plots representing spindle orientation over time were generated in R. Dot plots were generated in R, with median and IQR overlaid on the data. All data was plotted, unless stated otherwise in the text.

ACKNOWLEDGMENTS

We would like to thank past and present members of the Baum lab, Charras lab, and Mao lab for advice on the project and for their help with the manuscript. We would also like to thank the funders who enabled this work: M.L. was funded by the Agency for Science, Technology and Research (Singapore) and supported by the Wellcome Trust Developmental and Stem Cell Biology PhD program. M.L., N.R., and B.B. received support from the MRC (MC_CF12266). B.B. and N.R. thank Cancer Research UK for program grant support (Grant no. C1529/A1734). B.B. also thanks the Biological Sciences Research Council (BBSRC) for support (Grants no. BB/J008532/1 and no. BB/K009001/1) and N.R. also thanks the BBSRC for support. G.C. is supported by a consolidator grant from the European Research Council (MolCellTissMech, agreement 647186). Y.M. is funded by a Medical Research Council Fellowship MR/L009056/1 and a UCL Excellence Fellowship. A.L. is supported by an EMBO long-term postdoctoral fellowship (no. 29-2016).

REFERENCES

Amano M, Ito M, Kimura K, Fukata Y, Chihara K, Nakano T, Matsuura Y, Kaibuchi K (1996). Phosphorylation and activation of myosin by Rho-associated kinase (Rho-kinase). *J Biol Chem* 271, 20246–20249.

Bosveld F, Markova O, Guirao B, Martin C, Wang Z, Pierre A, Balakireva M, Gague I, Ainslie A, Christophorou N, et al. (2016). Epithelial tricellular junctions act as interphase cell shape sensors to orient mitosis. *Nature* 530, 495–498.

Brand AH, Perrimon N (1993). Targeted gene expression as a means of altering cell fates and generating dominant phenotypes. *Development* 118, 401–415.

Calleja M, Herranz H, Estella C, Casal J, Lawrence P, Simpson P, Morata G (2000). Generation of medial and lateral dorsal body domains by the pannier gene of *Drosophila*. *Development* 127, 3971–3980.

Campinho P, Behrndt M, Ranft J, Risler T, Minc N, Heisenberg C-P (2013). Tension-oriented cell divisions limit anisotropic tissue tension in epithelial spreading during zebrafish epiboly. *Nat Cell Biol* 15, 1405–1414.

Carreno S, Kouranti I, Glusman ES, Fuller MT, Echard A, Payre F (2008). Moesin and its activating kinase slik are required for cortical stability and microtubule organization in mitotic cells. *J Cell Biol* 180, 739–746.

Corrigan AM, Shrestha R, Draviam VM, Donald AM (2015). Modeling of noisy spindle dynamics reveals separable contributions to achieving correct orientation. *Biophys J* 109, 1398–1409.

Curran S, Strandkvist C, Bathmann J, de Gennes M, Kabla A, Salbreux G, Baum B (2017). Myosin II controls junction fluctuations to guide epithelial tissue ordering. *Dev Cell* 43, 480–492.e6.

Dimitracopoulos A, Lam M, Baum B (2016). Oriented division: using T-junctions to determine direction. *Curr Biol* 26, R371–R373.

di Pietro F, Echard A, Morin X (2016). Regulation of mitotic spindle orientation: an integrated view. *EMBO Rep* 17, 1106–1130.

Dujardin DL, Vallee RB (2002). Dynein at the cortex. *Curr Opin Cell Biol* 14, 44–49.

Fernandez P, Maier M, Lindauer M, Kuffer C, Storchova Z, Bausch AR (2011). Mitotic spindle orients perpendicular to the forces imposed by dynamic shear. *PLoS One* 6, e28965.

Finegan TM, Na D, Cammarota C, Skeeters AV, Nadasi T, Dawney NS, Fletcher AG, Oakes PW, Bergstralh DT (2018). Tissue tension and not interphase cell shape determines cell division orientation in the *Drosophila* follicular epithelium. *EMBO J* 1–18.

Fink J, Carpi N, Betz T, Bétard A, Chebah M, Azioune A, Bornens M, Sykes C, Fetler L, Cuvelier D, et al. (2011). External forces control mitotic spindle Positioning. *Nat Cell Biol* 13, 771–778.

Georgiou M, Baum B (2010). Polarity proteins and Rho GTPases cooperate to spatially organise epithelial actin-based protrusions. *J Cell Sci* 123, 1089–1098.

Gibson WT, Gibson MC (2009). Cell topology, geometry, and morphogenesis in proliferating epithelia. *Curr Top Dev Biol* 89, 87–114.

Gibson WT, Veldhuis JH, Rubinstein B, Cartwright HN, Perrimon N, Wayne Brodland G, Nagpal R, Gibson MC (2011). Control of the mitotic cleavage plane by local epithelial topology. *Cell* 144, 427–38.

Gloerich M, Bianchini JM, Siemers KA, Cohen DJ, James Nelson W (2017). Cell division orientation is coupled to cell–cell adhesion by the E-cadherin/LGN complex. *Nat Commun* 8, 13996.

Grill SW, Hyman AA (2005). Spindle positioning by cortical pulling forces. *Dev Cell* 8, 461–465.

Hart KC, Tan J, Siemers KA, Sim JY, Pruitt BL, Nelson WJ, Gloerich M (2017). E-cadherin and LGN align epithelial cell divisions with tissue tension independently of cell shape. *Proc Natl Acad Sci USA* 114, E5845–E5853.

Heppert JK, Pani AM, Roberts AM, Dickinson DJ, Goldstein B (2018). A CRISPR tagging-based screen reveals localized players in Wnt-directed asymmetric cell division. *Genetics* 208, 1147–1164.

Hertwig O (1896). *The Biological Problem of To-Day Preformation or Epigenesis? The Basis of a Theory of Organic Development*, ed. W Heinemann (translated), London: Heinemann's Scientific Handbooks.

Kimura K, Kimura A (2011). A novel mechanism of microtubule length-dependent force to pull centrosomes toward the cell center. *BioArchitecture* 1, 74–79.

Kotak S, Gönczy P (2013). Mechanisms of spindle positioning: cortical force generators in the limelight. *Curr Opin Cell Biol* 16, 1–8.

Kraft LM, Lackner LL (2017). Mitochondria-driven assembly of a cortical anchor for mitochondria and dynein. *J Cell Biol* 216, 3061–3071.

Machicoane M, de Frutos CA, Fink J, Rocancourt M, Lombardi Y, Gare S, Piel M, Echard A (2014). SLK-dependent activation of ERMs controls LGN–NuMA localization and spindle orientation. *J Cell Biol* 205, 791–799.

Mao Y, Tournier AL, Bates PA, Gale JE, Tapon N, Thompson BJ (2011). Planar polarization of the atypical myosin Dachs orients cell divisions in *Drosophila*. *Genes Dev* 25, 131–136.

Mao Y, Tournier AL, Hoppe A, Kester L, Thompson BJ, Tapon N (2013). Differential proliferation rates generate patterns of mechanical tension that orient tissue growth. *EMBO J* 32, 2790–2803.

Marinari E, Mehonic A, Curran S, Gale J, Duke T, Baum B (2012). Live-cell delamination counterbalances epithelial growth to limit tissue over-crowding. *Nature* 484, 542–545.

- Matsumura S, Kojidani T, Kamioka Y, Uchida S, Haraguchi T, Kimura A, Toyoshima F (2016). Interphase adhesion geometry is transmitted to an internal regulator for spindle orientation via caveolin-1. *Nat Commun* 7, ncomms11858.
- Minc N, Burgess D, Chang F (2011). Influence of cell geometry on division-plane positioning. *Cell* 144, 414–426.
- Minc N, Piel M (2012). Predicting division plane position and orientation. *Trends Cell Biol* 22, 193–200.
- Mizuno T, Amano M, Kaibuchi K, Nishida Y (1999). Identification and characterization of *Drosophila* homolog of Rho-kinase. *Gene* 238, 437–444.
- Nakajima Yu-I, Kuranaga E, Sugimura K, Miyawaki A, Miura M (2011). Nonautonomous apoptosis is triggered by local cell cycle progression during epithelial replacement in *Drosophila*. *Mol Cell Biol* 31, 2499–2512.
- Nestor-Bergmann A, Stooke-Vaughan GA, Goddard GK, Starborg T, Jensen OE, Woolner S (2017). Decoupling the roles of cell shape and mechanical stress in orienting and cueing epithelial mitosis. *Cell Rep* 26, 2088–2100.e4.
- O’Connell CB, Wang Y-L (2000). Mammalian spindle orientation and position respond to changes in cell shape in a dynein-dependent fashion. *Mol Biol Cell* 11, 1765–1774.
- Oakes PW, Banerjee S, Cristina Marchetti M, Gardel ML (2014). Geometry regulates traction stresses in adherent cells. *Biophys J* 107, 825–833.
- Radulescu AE, Cleveland DW (2010). NuMA after 30 years: the matrix revisited. *Trends Cell Biol* 20, 214–222.
- Ramkumar N, Baum B (2016). Coupling changes in cell shape to chromosome segregation. *Nat Rev Mol Cell Biol* 17, 511–521.
- Redemann S, Pecreaux J, Goehring NW, Khairy K, Stelzer EHK, Hyman AA, Howard J (2010). Membrane invaginations reveal cortical sites that pull on mitotic spindles in one-cell *C. elegans* embryos. *PLoS One* 5, e12301.
- Rosa A, Vlassaks E, Pichaud F, Baum B (2015). Ect2/Pbl acts via Rho and polarity proteins to direct the assembly of an isotropic actomyosin cortex upon mitotic entry. *Dev Cell* 604–616.
- Scarpa E, Finet C, Blanchard GB, Sanson B (2018). Actomyosin-driven tension at compartmental boundaries orients cell division independently of cell geometry in vivo. *Dev Cell* 47, 727–740.e6.
- Tang Z, Hu Y, Wang Z, Jiang K, Zhan C, Marshall WF, Tang N (2018). Mechanical forces program the orientation of cell division during airway tube morphogenesis. *Dev Cell*, 44, 313–325.e5.
- Théry M, Jiménez-Dalmaroni A, Racine V, Bornens M, Jülicher F (2007). Experimental and theoretical study of mitotic spindle orientation. *Nature* 447, 493–496.
- Théry M, Racine V, Pépin A, Piel M, Chen Y, Sibarita J-B, Bornens M (2005). The extracellular matrix guides the orientation of the cell division axis. *Nat Cell Biol* 7, 947–953.
- Théry M, Racine V, Piel M, Pepin A, Dimitrov A, Chen Y, Sibarita J-B, Bornens M (2006). Anisotropy of cell adhesive microenvironment governs cell internal organization and orientation of polarity. *Proc Natl Acad Sci USA* 103, 19771–19776.
- Wilson EB (1925). *The Cell in Development and Inheritance*. New York, London: Macmillan and Co.
- Winter CG, Wang B, Ballew A, Royou A, Karess R, Axelrod JD, Luo L (2001). *Drosophila* Rho-associated kinase (Drok) links frizzled-mediated planar cell polarity signaling to the actin cytoskeleton. *Cell* 105, 81–91.
- Wühr M, Tan ES, Parker SK, Detrich HW, Mitchison TJ (2010). A model for cleavage plane determination in early amphibian and fish embryos. *Curr Biol* 20, 2040–2045.
- Wyatt TPJ, Harris AR, Lam M, Cheng Q, Bellis J, Dimitracopoulos A, Kabla AJ, Charras GT, Baum B (2015). Emergence of homeostatic epithelial packing and stress dissipation through divisions oriented along the long cell axis. *Proc Natl Acad Sci USA* 112, 5726–5731.
- Zitserman D, Roegiers F (2011). Live-cell imaging of sensory organ precursor cells in intact *Drosophila* pupae. *J Vis Exp* 51.